Direct and Reliable Patterning of Plasmonic Nanostructures with Sub-10-nm Gaps

Huigao Duan,[†] Hailong Hu,[‡] Karthik Kumar,[†] Zexiang Shen,[‡] and Joel K. W. Yang[†,*]

[†]Institute of Materials Research and Engineering, A*STAR (Agency for Science, Technology and Research), 3 Research Link, 117602 Singapore and [‡]School of Physical and Mathematical Sciences, Nanyang Technological University, 21 Nanyang Link, 637371 Singapore

ABSTRACT Nanoscale gaps in metal films enable strong field enhancements in plasmonic structures. However, the reliable fabrication of ultrasmall gaps (<10 nm) for real applications is still challenging. In this work, we report a method to directly and reliably fabricate sub-10-nm gaps in plasmonic structures without restrictions on pattern design. This method is based on a lift-off process using high-resolution electron-beam lithography with a negative-tone hydrogen silsesquioxane (HSQ) resist, where the resulting nanogap size is determined by the width of the patterned HSQ structure, which could be written at less than 10 nm. With this method, we fabricated densely packed gold nanostructures of varying geometries separated by ultrasmall gaps. By controlling structure sizes during lithography with nanometer precision, the plasmon resonances of the resulting patterns could be accurately tuned. Optical and surface-enhanced Raman scattering (SERS) measurements on the patterned structures show that this technique has promising applications in the fabrication of passively tunable plasmonic nanostructures with ultrasmall gaps.

KEYWORDS: sub-10-nm gaps · plasmon resonance · field enhancement · lift-off · SERS

Plasmon resonances occurring in metal nanostructures separated by nanometer-sized gaps can result in strong electric fields in sub-diffraction-limited volumes.[1,2] The energy focusing effect of these tiny gaps has been observed to intensify with decreasing gap size. For instance, field enhancements by orders of magnitude have been demonstrated in sub-10-nm gaps in gold structures.[3,4] This large field enhancement shows promising applications in surface-enhanced spectroscopy,[5,6] nonlinear optics,[7] optical rectification,[8] and heat-assisted magnetic recording.[9] Additionally, strong plasmon coupling occurring between closely spaced plasmonic structures[10,11] gives rise to energy splitting of resonant modes.[12] This coupling enables large shifts in resonant energies that occur with miniscule changes in the environment and/or the gap size of the plasmonic structures,[13] hence making them useful in high-sensitivity chemical detection[14] and plasmonic nanorulers.[15]

The fabrication of nanogaps with well-defined dimensions and large-area uniformity in plasmonic structures is crucial for their use in real applications. Although much work has been done to understand plasmon resonances in metal nanostructures with ultrasmall gaps,[10] it is still challenging to reliably fabricate them. Currently, sub-10-nm gaps between metal nanostructures are often fabricated by indirect approaches such as edge lithography,[16] angled deposition methods,[17] clustering of chemically synthesized nanoparticles,[18−20] breakage of constricted wires due to electromigration,[8,21] and on-wire lithography.[22,23] However, these methods are limited either in their yield or in the variety of patterns achievable. To achieve greater freedom in pattern design, we need a direct method for fabricating these nanogaps. Simultaneously, the method should also enable high-density patterning of uniform structures over large areas, which will be useful in experiments and applications.

In this article, we present a method that enables the direct and reliable fabrication of sub-10-nm gaps between plasmonic nanostructures. The method is based on a high-resolution electron-beam lithography process with a negative-tone hydrogen silsesquioxane (HSQ) resist followed by lift-off. As the HSQ structures can be patterned at sub-10-nm line widths,[24,25] it was advantageous to have these structures determine the nanogap dimensions. We demonstrated that, with the HSQ lift-off process, densely packed gold nanostructures were fabricated with gaps as small as 5 nm. Optical measurements and finite-difference time-domain (FDTD) simulations showed that these ordered structures with small gaps have promising plasmonic properties and potential for surface-enhanced Raman scattering (SERS) applications.

RESULTS AND DISCUSSION

Fabrication. Given that lift-off processes are usually achieved using positive-tone

* Address correspondence to yangkwj@imre.a-star.edu.sg.

Received for review July 11, 2011 and accepted August 16, 2011.

Published online August 16, 2011
10.1021/nn2025868

resists, we first show a comparison between the use of a negative-tone and a positive-tone resist for lift-off particularly in the patterning of nanogaps in metal nanostructures. Figure 1a shows the process flow using HSQ (negative-tone) lift-off. The details of the process can be found in the Methods section. Briefly, a thin HSQ layer was first spin-coated onto a silicon substrate and exposed using an electron beam. After development, metal was deposited onto the sample. Finally, metal nanostructures with small gaps were obtained by lift-off. In comparison to the more common lift-off process with positive resist (*e.g.*, PMMA[26]) in Figure 1b, the HSQ process required less amount of electron-beam exposure and resulted in resist structures that were mechanically and thermally stable. Furthermore, as the distance between electron-beam paths was larger in the HSQ process, the exposure profiles were sharper due to less electron proximity effects,[27] hence resulting in high-resolution resist structures with straight side walls which are desirable for lift-off.

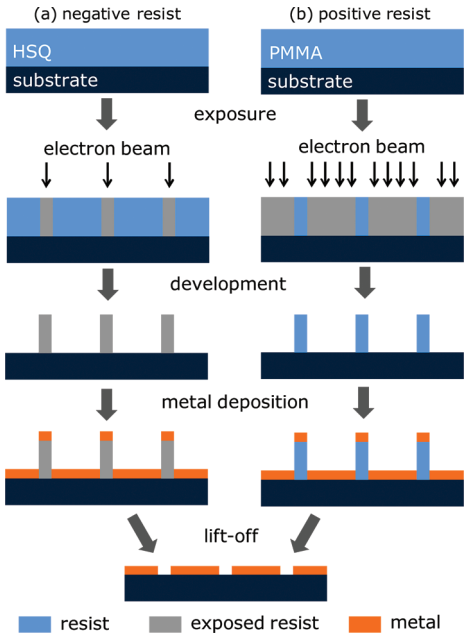

Figure 1. Comparison of lift-off process using a negative-tone resist (*e.g.*, HSQ) and a positive-tone resist (*e.g.*, PMMA) to fabricate dense metal structures separated by small gaps. In this particular example, using a negative-tone resist will require electron-beam exposure over a smaller area, which could lead to higher throughput.

Figure 2 shows schematics and scanning electron micrographs (SEM) at various stages of the process. A small area of a representative pattern layout used for electron-beam lithography is shown in Figure 2a, in which single-pixel lines in red form a hexagonally networked pattern with 30 nm edge lengths. Figure 2b shows a SEM image of the resulting HSQ pattern after exposure and development. The line width of HSQ structures was ~5 nm (see also Figure S1 in the Supporting Information for TEM inspection results), and the structures were ~150 nm tall. Despite the high aspect ratio of >20, the structures remained upright due to the sufficient mechanical strength of the material when they form interconnected structures. For comparison, isolated structures of the same aspect ratio would most likely have fallen over.[28,29] Figure 2c shows a SEM image of the structures after the deposition of 15 nm Au (with 1 nm Cr adhesion layer) by electron-beam evaporation. Due to finite lateral deposition[30] of Au, as shown schematically in the inset,

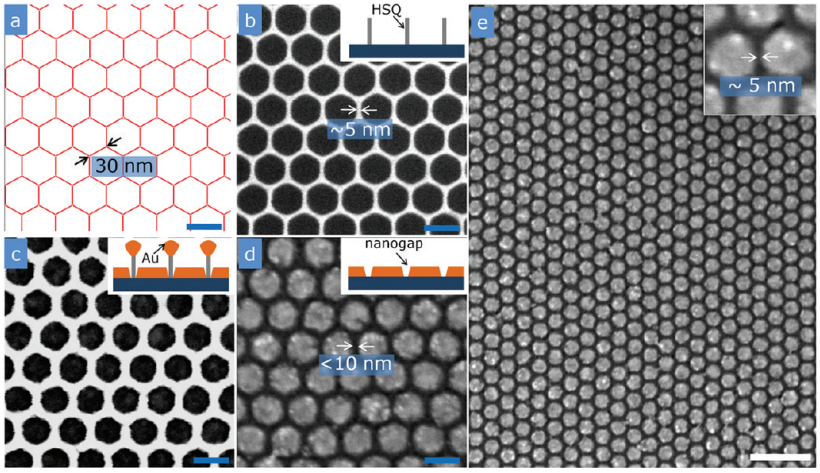

Figure 2. Results from the fabrication of Au structures with sub-10-nm gaps using HSQ-based lift-off process. (a) Layout consisting of single-pixel lines for electron-beam lithography. (b) SEM image of HSQ high aspect ratio networking structures after exposure and development, showing the line width of HSQ structures was ~5 nm. The inset is a schematic showing the cross section of high aspect ratio structures. (c) HSQ structures after electron-beam evaporation of 15 nm gold, showing that the structures increased to ~10 nm due to lateral growth. The inset shows the possible cross sections of the structures. (d) Gold nanodisk array after removal of HSQ by HF lift-off. The inset shows the possible side wall profile of the formed nanogaps, indicating trapezoidal cross section. (e) Low-magnification SEM image showing a large array of gold nanodisks with ~10 nm gaps fabricated using the HSQ-based lift-off process. The initial HSQ thickness was 150 nm. Electron-beam lithography was performed with an Elionix system with an accelerating voltage of 100 kV. The dose for HSQ exposure was 16 nC/cm. Scale bars: (a–d) 50 nm; (e) 200 nm.

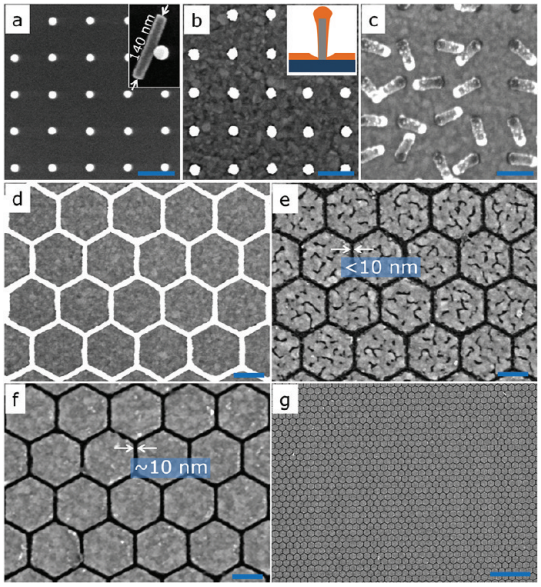

Figure 3. (a–c) SEM images showing the side wall deposition effect on the lift-off process: (a) 140 nm tall and 100 nm pitch HSQ pillars. The inset image includes a collapsed HSQ pillar, showing the vertical side wall of the HSQ pillars. (b) HSQ pillars after 15 nm gold evaporation. The inset is a schematic showing the possible cross-section profile (a thin coating layer) of the pillars caused by side wall deposition of gold. (c) Structures after HF rinse, showing that gold structures with a tubular shape remained on the surface, which indicates the side wall deposition of gold onto the HSQ pillars. (d–f) SEM images of HSQ-based lift-off results with different HSQ or gold layer thickness: (d) 100 nm thick HSQ and 15 nm thick gold layer, showing an unsuccessful lift-off; (e) 100 nm thick HSQ with 10 nm thick gold layer, showing a successful lift-off to fabricate sub-10-nm gaps; (f) 150 nm thick HSQ with 15 nm thick gold layer, showing a successful lift-off to fabricate ~10 nm gaps in gold nanodisks. (g) Low-magnification SEM image showing a large area hexagonal nanodisk array fabricated using the parameters in (f). All initial HSQ structures were hexagonally networked with a line width of ~6 nm and an edge length of 100 nm. Electron-beam lithography and SEM imaging parameters were similar to Figure 2. Scale bars: (a–f) 100 nm, and (g) 1 μm.

the HSQ structures with Au overcoat have widened to ~10 nm. These Au-coated HSQ structures were removed during lift-off, resulting in gold nanodisk structures separated by ~10 nm gaps, as seen in Figure 2d. Although the gap size on the top of the Au structures was ~10 nm, the gaps at the base of the structures were ~5 nm as defined by the width of the HSQ structures, resulting in a cross-sectional profile as illustrated in the inset of Figure 2d. Figure 2e is a SEM image of a large array of gold nanodisks, showing uniformly defined nanodisks with sub-10-nm gaps.

As alluded to above, gold deposition on the side walls of HSQ structures was the main obstacle to achieving successful lift-off. Examples of unsuccessful lift-off can be clearly seen in isolated structures, as shown in Figure 3a–c. Figure 3a is a SEM of a HSQ pillar array with a pitch of 100 nm. An enlarged view of a collapsed HSQ pillar with straight parallel side walls is shown in the inset. Figure 3b shows the structures after 15 nm Au deposition. An attempted but unsuccessful lift-off resulted in collapsed pillar structures, as shown in Figure 3c. Upon closer inspection, we observed nanometer-sized clusters of Au on the walls of these collapsed structures. The HSQ within these Au shells appears to have been dissolved away during the lift-off, but the continuous thin side wall coating connecting the top Au cap with the film on the substrate prevented the complete removal of Au. This thin side wall coating was a result of off-normal arrival of Au atoms, which in turn could be the effect of not having a perfect point source during the metal evaporation. Ultrasonic agitation was therefore necessary to perform successful lift-off in the presence of side wall coating to mechanically break off the Au-coated HSQ structures from the film on the substrate.

Given the constraints of the deposition tool, we aimed to weaken the metal coating on the side walls to achieve successful lift-off by (1) reducing the thickness of gold deposition to decrease the total thickness of the side wall coating, and (2) increasing the height of HSQ structures to obtain a thinner side wall coating near the film on the substrate. The effects of these methods are shown in Figure 3d–f. All initial HSQ structures in Figure 3d–f were hexagonally networked with ~6 nm line width and 100 nm edge length. Figure 3d shows a SEM image from an unsuccessful lift-off process, in which we used a ~100 nm thick HSQ resist (instead of 150 nm as used to obtain results in Figure 2) and deposited a ~15 nm thick gold layer. However, when we decreased the thickness of gold layer to 10 nm while keeping other parameters constant, successful lift-off was achieved, as shown in Figure 3e, though with discontinuous structures within each cell due to insufficient Au thickness. The effect of resist thickness can be seen as increasing the resist thickness to 150 nm, while keeping the metal thickness at 15 nm led to successful lift-off, as shown in Figure 3f and in Figure 2d,e. Figure 3g shows a low-magnification SEM image of the array of hexagonal gold plates separated by ~10 nm gaps. In our experiments, no defects were found in gold nanostructures over the entire patterned area (12 μm × 12 μm), as also shown in the Supporting Information Figures S2 and S3.

One main advantage of this direct patterning approach is the freedom it affords in designing plasmonic structures of various shapes and sizes. For example, with this HSQ-based lift-off process, different shapes of gold nanostructures with small gaps were fabricated, for example, squares in Figure 4a and triangles in Figure 4b. At the expense of exposing a larger fraction of the patterned area, we could also directly pattern sparser structures such as bowtie nanoantennas and trimers, which are useful also in focusing optical energy into their nanogaps.[2,31] Such structures are shown in Figure 4c,d, where ~10 nm gaps at the center of the groups of triangles could be reliably achieved. In comparison to a high-resolution PMMA-based lift-off

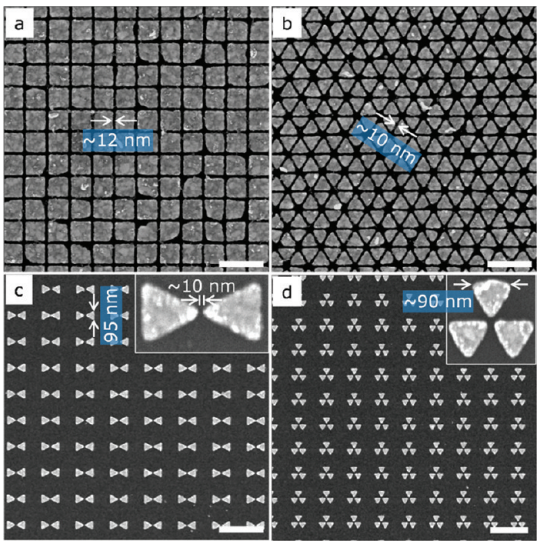

Figure 4. SEM images of different types of gold nanostructures with ~10 nm gaps fabricated by HSQ-based lift-off process on the silicon substrate. (a) Gold squares with 100 nm pitch. The average edge length of the gold squares was ~90 nm. (b) Hexagonally distributed gold nanotriangles with 100 nm pitch. The average edge length of them was about ~70 nm. (c) Gold bowtie nanostructures with an edge length of ~95 nm. (d) Gold trimer structures with an average triangle edge length of ~90 nm. The thickness of HSQ used here for lift-off was ~150 nm. All gold structures were 15 nm thick with a 1 nm Cr adhesion layer on the bottom. Scale bars: (a,b) 200 nm; (c,d) 500 nm.

process (see Figure S4), we observed a qualitative improvement in uniformity of the gap dimensions.

Plasmonic Activity of the Fabricated Structures. The plasmonic activity of the fabricated gold nanostructures was observed by measuring their optical extinction spectra (see Methods section for more details). The measurements presented here were performed on gold nanostructures with 200 nm pitch and 30 nm thickness, achieved using HSQ-based lift-off with 180 nm thick HSQ resist. Due to the higher thickness of gold used here, that is, 30 nm instead of 15 nm, the observed minimum gap size at the top of the structures was correspondingly larger at ~15 nm.

Figure 5a shows the extinction spectra for arrays of gold nanosquares with different gaps from 30 to 15 nm (see Figure S5 for the corresponding SEM images), while keeping the pitch constant at 200 nm. The edge length of the structures was therefore varied from 170 to 185 nm. From Figure 5a, we observe three plasmon resonance peaks for each array of Au nanostructures as indicated by I, II, and III. Their resonance peaks were observed to significantly red shift when the gap was decreased, suggesting the tunability of the plasmon resonance wavelength of the array. This shift was as expected because larger structures and smaller gaps have both been observed to cause red shifts in the plasmon resonance peaks.[32] To identify the corresponding plasmon resonance modes for each peak and observe the resonance shift in the structures, we

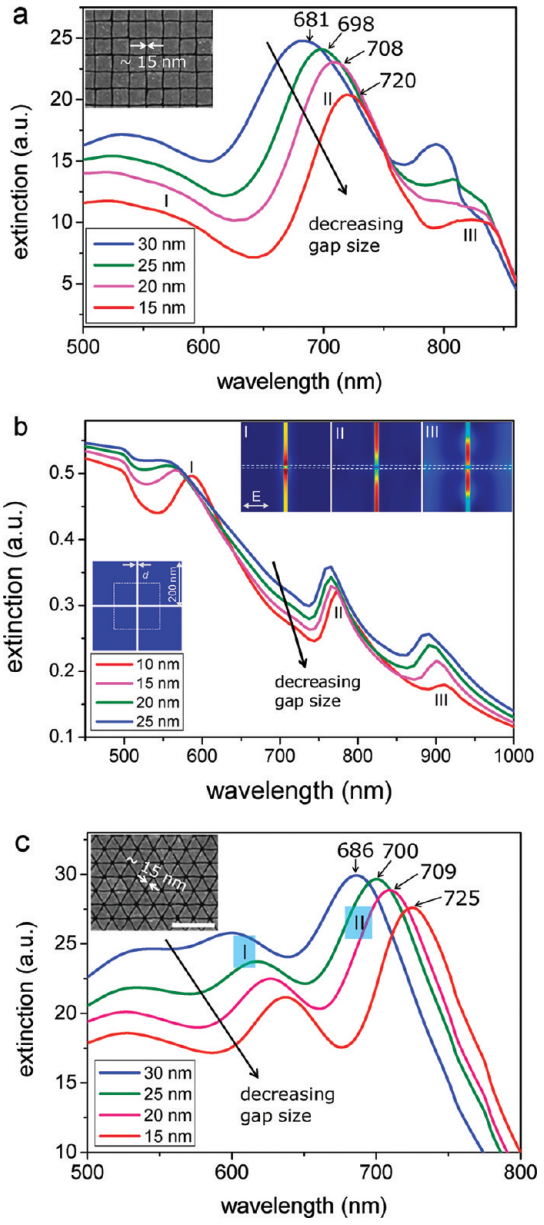

Figure 5. Extinction spectra for densely packed gold nanostructures with different gap sizes on a silicon substrate: (a) experimental spectra for the nanosquare array; (b) simulated spectra for the nanosquares. (Inset) Near-field distributions for each plasmon resonance mode within a unit cell of the periodic array; (c) experimental spectra for the nanotriangle array. These spectra show that plasmon resonance energies could be tuned by changing the shapes and the gap size/nanostructureparticle size of the pattern, indicating also that these structures with small gaps as fabricated with the HSQ-based lift-off process were plasmonically active. The HSQ thickness here for lift-off was ~180 nm. The thickness of gold was 30 nm. The pitch between gold nanoparticles was 200 nm. The small box with dashed lines in (b) is the unit cell for periodic boundary conditions in numerical simulations. The dashed lines in the field plots in (b) show the boundary of the squares. Scale bars in SEM images: 500 nm.

performed finite-difference time-domain (FDTD) simulations (see Methods). The results are shown in Figure 5b, from which we can see three distinct peaks in the spectra that red shift when decreasing the gap

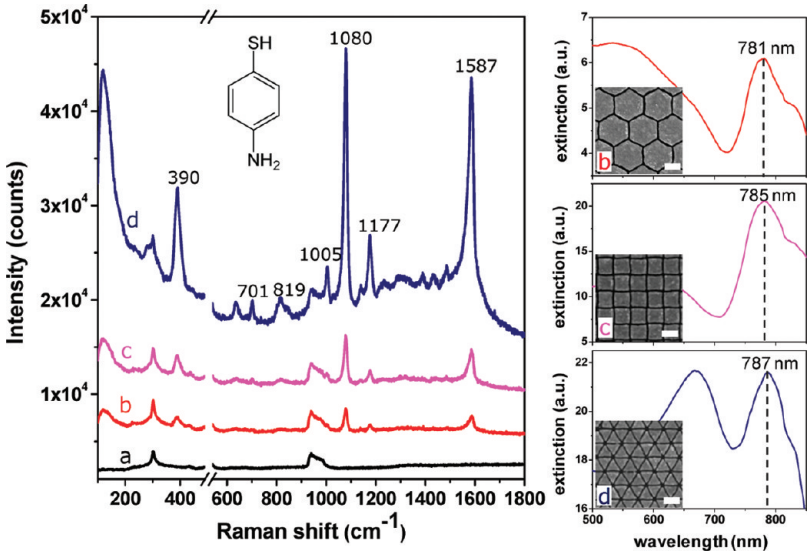

Figure 6. SERS spectra of 4-ATP absorbed on the densely packed gold nanostructures with different shapes on the silicon substrate: (a) gold film without nanogaps; (b) nanohexagons; (c) nanosquares; (d) nanotriangles. The results show that nanotriangles had the best enhancement factor. All Au nanoparticles were fabricated using HSQ-based lift-off technique with same pitch of ~200 nm, thickness of ~22 nm, and gap size of ~15 nm, as shown by the SEM images. The Au nanoparticles also had a similar plasmon resonance peak ~785 nm which was the excitation wavelength for the SERS measurement. The SERS was done on a Renishaw inVia Raman microscope with intensity of 0.6 mW and integration time of 30 s. The break from 490 and 540 nm is intentionally introduced to erase the silicon (100) peak. Scale bars in SEM images: 200 nm.

size, which qualitatively agree with experiment. The simulation was also able to produce the similar decrease in the height of peak III when the gap was made smaller as was observed experimentally. While qualitative agreement was good, we did not attempt to achieve quantitative agreement, which we believe could be attained by fine adjustment the material dielectric constants and modifying the structure geometries to match those obtained experimentally. The near-field distributions for each mode are shown in the inset, with each pattern corresponding to a different plasmon mode. However, a detailed understanding of the resulting charge distributions is beyond the scope of this paper and will be a topic for future studies.

The tunability of the plasmon resonance energies was also observed in the case of Au nanotriangle array as shown in Figure 5c. In contrast to the nanosquare array, the nanotriangle array showed two dinstinct plasmon resonance peaks in the range of wavelengths measured, as indicated by I and II in Figure 5c. The presence of resonance peaks in the extinction spectra indicated that these densely packed structures were also plasmonically active and that their resonances were tunable by adjusting the fabrication parameters. Further evidence of plasmonic activity of these structures can be found in Figure S6, where the polarization-dependent plasmon resonances are shown in gold nanorectangles with ultrasmall gaps.

Surface-Enhanced Raman Scattering. A promising application of plasmonic nanostructures with ultrasmall gaps is in surface-enhanced Raman scattering (SERS). One of the requirements to achieve strong SERS signal is the spectral alignment of the excitation laser with the plasmon resonance of the plasmonic system.[33] Taking advantage the direct-patterning process, we finely tuned the resonance frequency to align the resonances for patterns of different shapes to the excitation wavelength. In addition to controlling the gap size, to match the 785 nm excitation laser that was used, we tuned the plasmon resonance of the densely packed gold nanostructures also by adjusting the thickness of the Au film to ~22 nm, as shown in the right side in Figure 6. Compared to the 30 nm thick gold nanostructures in Figure 5, a thinner gold film resulted in a red shift in the plasmon resonance of structures with the same dimension and gap size, hence enabling the shift from 708 to 785 nm. The corresponding plasmon resonance wavelengths of gold nanohexagons and nanotriangles were 781 and 787 nm, respectively. The size of nanogaps in these structures was kept constant at ~15 nm. A monolayer of 4-aminothiophenol (4-ATP) molecules was used as the probe for SERS measurement. The details for the preparation of the SERS substrate can be found in the Methods section.

The SERS results are also shown in Figure 6. As shown in spectrum a, for the unpatterned region of the sample (*i.e.*, bare gold film on Si), we were unable to detect any enhanced Raman scattering signal from the 4-ATP molecules. However, for the nanostructures with small gaps, strong Raman signals with clear peaks were observed, as shown in spectra b–d. As the concentration of the molecules in the detection region was same on both patterned and unpatterned areas (since the measurements were done on the same substrate), the enhanced Raman scattering was due to the field

enhancement in the small gaps afforded by plasmon resonance.

Perhaps most interesting was the observation that the enhancement factor (EF) of different gold nanostructures was highly dependent on the shapes of nanostructures. Taking the peak of 1080 cm^{-1} as an example, the signals from nanosquares and nanotriangles were ~2 and ~11 times higher, respectively, compared to the Raman signal from nanohexagons. As the shape of the structures was the only parameter that was varied, with all other parameters (substrate, gap size, excitation wavelength, and plasmon resonance frequency) kept constant, the different EFs were a manifestation of the shape effect of nanostructures. One possible effect of the structure shape was the increasing number of molecules in the nanogaps when going from hexagons to squares and triangles. Given that the molecules have self-assembled into a monolayer, the number of molecules in the gaps was roughly proportional to the total surface area available to the molecules at the nanogaps, which was conservatively estimated to be in the ratio of 1 (hexagons):1.7 (squares):3 (triangles). However, this effect alone cannot explain the large Raman enhancement observed from Au nanotriangles, which points to a further plasmonic field enhancement effect that is related to the shape. We explain this shape effect as follows: the nanotriangles, with sharper corners than the squares and hexagons, were more effective in generating strong fields that were confined at the corners due to the "lightning rod" effect.[34] To support this claim, the plots of field distributions in the case of nanotriangle arrays (Figure S7) appear to be the only ones with highly localized electric field maxima located at the corners of the structures. We hypothesize that these "hot spots" were responsible for the largest SERS signals for nanotriangles over nanosquares and nanohexagons. In contrast, the electric fields for nanohexagons and nanosquares were more delocalized compared to those for nanotriangles.

CONCLUSIONS

We demonstrated the direct and reliable patterning of arrays of plasmonic structures separated by sub-10-nm gaps. The method developed was based on a lift-off process using high-resolution electron-beam lithography with a negative-tone HSQ resist, where the resulting nanogap size was determined by the width of the patterned HSQ structure, which could be as small as ~5 nm. Optical measurements show that this process provided a powerful capability in the fabrication of tunable plasmonic nanostructures with ultrasmall gaps. With this technique, we studied the shape effect of nanostructures in achieving strong SERS signals in a systematic way and showed that arrays of nanotriangles were better than squares or hexagons. In addition to plasmonics, this high-resolution approach for patterning sub-10-nm gaps can be extended to the fabrication of nanostructures in other materials as well, such as nanochannels in nanofluidics, nanomagnets for magnetic interaction studies and gaps in metal for molecular electronics,[35] and dielectrophoretic trapping of particles.[36]

METHODS

Electron-Beam Lithography. HSQ (XR-1541-006, Dow Corning, USA) was spin-coated on silicon substrates with a thickness from 100 to 180 nm (measured by ellipsometry). To avoid thermally induced cross-linking which would reduce the resolution, no baking process was utilized. Electron-beam lithography was performed using an Elionix ELS-7000 EBL system with an accelerating voltage of 100 kV and a beam current of 100 pA. Depending on the density of the structures, typical doses to obtain HSQ structures with ~5 nm feature size were varied from 10 to 20 nC/cm. Exposed HSQ was developed in a salty developer (1% NaOH + 4% NaCl in DI water) at 24 °C for 4 min and then rinsed by DI water for 2 min to stop the development and clean the sample surface.[37] The samples were then directly rinsed with IPA. As IPA has a lower surface tension than DI water, this process reduced the probability of structure collapse by weakening the capillary force during the drying step.[38] The samples were blown dry using a steady stream of N_2.

Metal Deposition. Metal deposition was performed using an electron-beam evaporator (Explorer Coating System, Denton Vacuum). Before Au layer deposition, a 1 nm Cr adhesion layer was deposited. The working pressure during the evaporation was $<5 \times 10^{-6}$ Torr. The temperature of the sample chamber was kept at 20 °C during the entire evaporation process, with the sample holder rotating at a rate of 50 rpm to ensure the uniformity of deposition.

Lift-Off. Lift-off was performed by immersing the samples in 1:5 buffered hydrofluoric acid (HF) solution (7:1 of 40% NH_4F and 49% HF) at room temperature with ultrasonic agitation for 4 min. We observed that sonication was essential for successful lift-off in our experiments. The fabricated structures were imaged using an Elionix ESM-9000 scanning electron microscope with an accelerating voltage of 10 kV and a working distance of 5 mm.

Optical Measurement. To investigate the optical property of the fabricated structures, extinction spectra were measured in reflection mode using a QDI 2010 UV–visible–NIR range microspectrophotometer (CRAIC Technology Inc.). Both the incident and the collected light were normal to the substrate; that is, the electric field of light was in plane with the surface of nanostructures.

FDTD Simulations. Full 3D finite-difference time-domain (FDTD) simulations were performed on a workstation using the commercial software Lumerical by Lumerical Solutions Inc., Vancouver, Canada. To obtain qualitative trends and distinct peaks in the spectra, we simplified the structures significantly; for example, no Cr adhesion was used in the simulations. Periodic boundary conditions were used for the two in-plane dimensions to simulate an infinite array of periodic nanosquares, nanotriangles, and nanohexagons with small gaps. Perfectly matched layer (PML) boundary conditions were used in the *z*-direction. The mesh size used in the simulation region was 1 nm. The complex dielectric constants for Au and Si were selected as CRC[39] and Palik[40] from the database, respectively. The structures were illuminated with a plane wave directed along the *z*-axis. Time-averaged total electric

field intensity was extracted for the spectra and in generating the field distributions.

Surface-Enhanced Raman Scattering (SERS). To prepare the substrate for SERS, the sample was first immersed in a solution of 4-aminothiophenol (4-ATP) in ethanol at a concentration of 10^{-5} M for 12 h. The sample was then rinsed several times with ethanol and blow-dried using a N_2 stream. The rinsing process ensured the formation of only a monolayer of 4-ATP over the surface of Au. The SERS measurements were performed using a Renishaw inVia Raman microscope equipped with 785 nm GaAs laser. Raman signal were collected using a 100× objective (numerical aperture, NA = 0.85) under laser power intensity of 0.6 mW and with integration time of 30 s.

Acknowledgment. This work was supported by the Agency of Science, Technology and Research (A*STAR) in Singapore. Patterning was done at SNFC's shared Elionix ELS-7000 SEBL system in A*STAR. We thank Dr. J. Deng and Dr. H. Liu for technical assistance.

Supporting Information Available: Complementary fabrication and simulations results are provided by the supporting Figures S1−S7. This material is available free of charge *via* the Internet at http://pubs.acs.org.

REFERENCES AND NOTES

1. Schuller, J. A.; Barnard, E. S.; Cai, W.; Jun, Y. C.; White, J. S.; Brongersma, M. L. Plasmonics for Extreme Light Concentration and Manipulation. *Nat. Mater.* **2010**, *9*, 193–204.
2. Koh, A. L.; Fernndez-Domnguez, A. I.; McComb, D. W.; Maier, S. A.; Yang, J. K. W. High-Resolution Mapping of Electron-Beam-Excited Plasmon Modes in Lithographically Defined Gold Nanostructures. *Nano Lett.* **2011**, *11*, 1323–1330.
3. Ward, D. R.; Halas, N. J.; Ciszek, J. W.; Tour, J. M.; Wu, Y.; Nordlander, P.; Natelson, D. Simultaneous Measurements of Electronic Conduction and Raman Response in Molecular Junctions. *Nano Lett.* **2008**, *8*, 919–924.
4. Imura, K.; Okamoto, H.; Hossain, M. K.; Kitajima, M. Visualization of Localized Intense Optical Fields in Single Gold−Nanoparticle Assemblies and Ultrasensitive Raman Active Sites. *Nano Lett.* **2006**, *6*, 2173–2176.
5. Lim, D. K.; Jeon, K. S.; Kim, H. M.; Nam, J. M.; Suh, Y. D. Nanogap-Engineerable Raman-Active Nanodumbbells for Single-Molecule Detection. *Nat. Mater.* **2010**, *9*, 60–67.
6. Wei, H.; Ratchford, D.; Li, X.; Xu, H.; Shih, C. K. Propagating Surface Plasmon Induced Photon Emission from Quantum Dots. *Nano Lett.* **2009**, *9*, 4168–4171.
7. Kim, S.; Jin, J.; Kim, Y. J.; Park, I. Y.; Kim, Y.; Kim, S. W. High-Harmonic Generation by Resonant Plasmon Field Enhancement. *Nature* **2008**, *453*, 757–760.
8. Ward, D. R.; Hüser, F.; Pauly, F.; Cuevas, J. C.; Natelson, D. Optical Rectification and Field Enhancement in a Plasmonic Nanogap. *Nat. Nanotechnol.* **2010**, *5*, 732–736.
9. Stipe, B. C.; Strand, T. C.; Poon, C. C.; Balamane, H.; Boone, T. D.; Katine, J. A.; Li, J. L.; Rawat, V.; Nemoto, H.; Hirotsune, A.; *et al.* Magnetic Recording at 1.5 Pb m^{-2} Using an Integrated Plasmonic Antenna. *Nat. Photonics* **2010**, *4*, 484–488.
10. Halas, N. J.; Lal, S.; Chang, W. S.; Link, S.; Nordlander, P. Plasmons in Strongly Coupled Metallic Nanostructures. *Chem. Rev.* **2011**, *111*, 3913–3961.
11. Hentschel, M.; Dregely, D.; Vogelgesang, R.; Giessen, H.; Liu, N. Plasmonic Oligomers: The Role of Individual Particles in Collective Behavior. *ACS Nano* **2011**, *5*, 2042–2050.
12. Prodan, E.; Radloff, C.; Halas, N. J.; Nordlander, P. A Hybridization Model for the Plasmon Response of Complex Nanostructures. *Science* **2003**, *302*, 419–422.
13. Jain, P. K.; Huang, W.; El-Sayed, M. A. On the Universal Scaling Behavior of the Distance Decay of Plasmon Coupling in Metal Nanoparticle Pairs: A Plasmon Ruler Equation. *Nano Lett.* **2007**, *7*, 2080–2088.
14. Liu, N.; Tang, M. L.; Hentschel, M.; Giessen, H.; Alivisatos, A. P. Nanoantenna-Enhanced Gas Sensing in a Single Tailored Nanofocus. *Nat. Mater.* **2011**, *10*, 631–636.
15. Liu, N.; Alivisatos, A. P.; Hentschel, M.; Weiss, Th.; Giessen, H. Three-Dimensional Plasmon Rulers. *Science* **2011**, *332*, 1407–1410.
16. Im, H.; Bantz, K. C.; Lindquist, N. C.; Haynes, C. L.; Oh, S. H. Vertically Oriented Sub-10-nm Plasmonic Nanogap Arrays. *Nano Lett.* **2010**, *10*, 2231–2236.
17. Theiss, J.; Pavaskar, P.; Echternach, P. M.; Muller, R. E.; Cronin, S. B. Plasmonic Nanoparticle Arrays with Nanometer Separation for High-Performance SERS Substrates. *Nano Lett.* **2010**, *10*, 2749–2754.
18. Fan, J. A.; Wu, C.; Bao, K.; Bardhan, R.; Halas, N. J.; Manoharan, V. N.; Nordlander, P.; Shvets, G.; Capasso, F. Self-Assembled Plasmonic Nanoparticle Clusters. *Science* **2010**, *328*, 1135–1138.
19. Liberman, V.; Yilmaz, C.; Bloomstein, T. M.; Somu, S.; Echegoyen, Y.; Busnaina, A.; Cann, S. G.; Krohn, K. E.; Marchant, M. F.; Rothschild, M. A. Nanoparticle Convective Directed Assembly Process for the Fabrication of Periodic Surface Enhanced Raman Spectroscopy Substrates. *Adv. Mater.* **2010**, *22*, 4298–4302.
20. Slaughter, L. S.; Wu, Y.; Willingham, B. A.; Nordlander, P.; Link, S. Effects of Symmetry Breaking and Conductive Contact on the Plasmon Coupling in Gold Nanorod Dimers. *ACS Nano* **2010**, *4*, 4657–4666.
21. Ward, D. R.; Grady, N. K.; Levin, C. S.; Halas, N. J.; Wu, Y.; Nordlander, P.; Natelson, D. Electromigrated Nanoscale Gaps for Surface-Enhanced Raman Spectroscopy. *Nano Lett.* **2007**, *7*, 1396–1400.
22. Qin, L.; Park, S.; Huang, L.; Mirkin, C. A. On-Wire Lithography. *Science* **2005**, *309*, 113–115.
23. Osberg, K. D.; Schmucker, A. L.; Senesi, A. J.; Mirkin, C. A. One-Dimensional Nanorod Arrays: Independent Control of Composition, Length, and Interparticle Spacing with Nanometer Precision. *Nano Lett.* **2011**, *11*, 820–824.
24. Yang, J. K. W.; Cord, B.; Duan, H. G.; Berggren, K. K.; Klingfus, J.; Nam, S.-W.; Kim, K. B.; Rooks, M. J. Understanding of Hydrogen Silsesquioxane Electron Resist for Sub-5-nm-Half-Pitch Lithography. *J. Vac. Sci. Technol., B* **2009**, *27*, 2622–2627.
25. Duan, H.; Manfrinato, V. R.; Yang, J. K. W.; Winston, D.; Cord, B. M.; Berggren, K. K. Metrology for Electron-Beam Lithography and Resist Contrast at the Sub-10nm Scale. *J. Vac. Sci. Technol., B* **2010**, *28*, H11–H17.
26. Koh, A. L.; McComb, D. W.; Maier, S. A.; Low, H. Y.; Yang, J. K. W. Sub-10-nm Patterning of Gold Nanostructures on Silicon-Nitride Membranes for Plasmon Mapping with Electron Energy-Loss Spectroscopy. *J. Vac. Sci. Technol., B* **2010**, *28*, C6O45–C6O49.
27. Chang, T. H. P. Proximity Effect in Electron Beam Lithography. *J. Vac. Sci. Technol.* **1975**, *12*, 1271–1275.
28. Duan, H.; Berggren, K. K. Directed Self-Assembly at the 10 nm Scale by Using Capillary-Force-Induced Nanocohesion. *Nano Lett.* **2010**, *10*, 3710–3716.
29. Duan, H.; Yang, J. K. W.; Berggren, K. K. Controlled Collapse of High-Aspect-Ratio Nanostructures. *Small* **2011**, DOI: 10.1002/smll.201100892.
30. Vazquez-Mena, O.; Sidler, K.; Savu, V.; Park, C. W.; Guillermo Villanueva, L.; Brugger, J. Reliable and Improved Nanoscale Stencil Lithography by Membrane Stabilization, Blurring, and Clogging Corrections. *IEEE Trans. Nanotechnol.* **2011**, *10*, 352–357.
31. Ko, K. D.; Kumar, A.; Fung, K. H.; Ambekar, R.; Liu, G. L.; Fang, N. X.; Toussaint, K. C. Nonlinear Optical Response from Arrays of Au Bowtie Nanoantennas. *Nano Lett.* **2011**, *11*, 61–65.
32. Ghosh, S. K.; Pal, T. Interparticle Coupling Effect on the Surface Plasmon Resonance of Gold Nanoparticles: From Theory to Applications. *Chem. Rev.* **2007**, *107*, 4797–4862.
33. Campion, A.; Kambhampati, P. Surface-Enhanced Raman Scattering. *Chem. Soc. Rev.* **1998**, *27*, 241–250.
34. Boyack, R.; Le Ru, E. C. Investigation of Particle Shape and Size Effects in SERS Using T-Matrix Calculations. *Phys. Chem. Chem. Phys.* **2009**, *11*, 7398–7405.
35. Strachan, D. R.; Smith, D. E.; Johnston, D. E.; Park, T. H.; Therien, M. J.; Bonnell, D. A.; Johnson, A. T. Controlled

Fabrication of Nanogaps in Ambient Environment for Molecular Electronics. *Appl. Phys. Lett.* **2005**, *86*, 043109.
36. Strobel, S.; Sperling, R. A.; Fenk, B.; Parak, W. J.; Tornow, M. Dielectrophoretic Trapping of DNA-Coated Gold Nanoparticles on Silicon Based Vertical Nanogap Devices. *Phys. Chem. Chem. Phys.* **2011**, *13*, 9973–9977.
37. Yang, J. K. W.; Berggren, K. K. Using High-Contrast Salty Development of Hydrogen Silsesquioxane for Sub-10-nm Half-Pitch Lithography. *J. Vac. Sci. Technol., B* **2007**, *25*, 2025–2029.
38. Ocola, L. E.; Tirumala, V. R. Nanofabrication of Super-High-Aspect-Ratio Structures in Hydrogen Silsesquioxane from Direct-Write E-Beam Lithography and Hot Development. *J. Vac. Sci. Technol., B* **2008**, *26*, 2632–2635.
39. Lide, D. R., Ed. *CRC Handbook of Chemistry and Physics*, 86th ed.; CRC Press: Boca Raton, FL, 2005.
40. Palik, E. D. *Handbook of Optical Constants of Solids*; Academic Press: New York, 1997.